https://doi.org/10.5194/egusphere-2022-1233
Preprint. Discussion started: 9 December 2022

When climate and human interactions threaten soil and water resources through hyper sedimentation: example of El Niño events (1978-2019 period), Poechos Reservoir, Northern Peru

Anthony Foucher[1], Sergio Morera[2,3,4], Michael Sanchez[2], Jhon Orrillo[2] & Olivier Evrard[1]

[1] Laboratoire des Sciences du Climat et de l'Environnement (LSCE-IPSL), UMR 8212 (CEA/CNRS/UVSQ), Université Paris-Saclay, 91191 Gif-sur-Yvette Cedex, France
[2] Instituto Geofísico del Perú, Calle Badajoz, 169, Lima, Peru
[3] Universidad Nacional Agraria La Molina, Av. La Molina, s/n, Lima, Peru
[4] Universidad Nacional Autónoma de Huanta, Jr. Manco Cápac, 497 Ayacucho, Peru

Correspondence to: Anthony Foucher (Anthony.foucher@lsce.ipsl.fr)

Abstract. Although Extreme El Niño Events (EENE) have always impacted hydrology in South America, their intensification by global warming and their association with changes in human activities and land cover may lead to the acceleration of sediment transfers in river systems and dam reservoirs. This situation may threaten soil and water resources in a region highly dependent on freshwater originating from large dams. In this study, we investigated the sediment sequence accumulated in the Poechos reservoir (Northern Peru) and provided a retrospective reconstruction of the interactions of El Niño-Southern Oscillation (ENSO), agricultural practices and vegetation cover changes on sediment dynamics (1978-2019). To this end, a sediment core was dated and characterized by physical and chemical analyses (e.g. scanner tomography, X-ray fluorescence, particle size analysis) for estimating the evolution of sedimentation rates and changes in sediment sources during the last five decades.

Sediment tracing results indicated the occurrence of changes in sediment sources associated with positive and negative phases of the Central and East Pacific Index (C and E index), with a greater contribution of the lowland dry forest biome in comparison to that of the Andean source to sediment during the warm periods (El Niño events, ENE), (mean contribution of 76%, up to 90% during the Coastal El Niño Events (CENE) of 2016-2017). Overall, the development of agriculture within the fluvial plains of the dry forest biome upstream of the Poechos dam induced an acceleration of sedimentation rates by 140 % after 1997, with an accumulation of coarser sediment in the reservoir during ENE and EENE.

This study suggests that the expansion of agriculture (e.g. agriculture in floodplains, deforestation) associated with a higher frequency of extreme rainfall events amplified the consequences of ENE, EENE and CENE on the quantity and quality of sediment transported by this river system, which will significantly decrease the lifespan of the dam reservoir essential to meet freshwater demands of the farmers and the populations living in this region.

Keywords: Sediment core, Extreme El Niño events, Sediment tracing, Land use change, Water resources, Agriculture expansion

https://doi.org/10.5194/egusphere-2022-1233
Preprint. Discussion started: 9 December 2022

1 Introduction

In many regions of the world, the conversion of natural ecosystems into agricultural land was observed during the last several decades to meet the local and global demand for food and other commodities of a growing population (Winkler et al., 2021). South-America is one of the most affected continents by this recent phase of agricultural expansion and land cover change (Song et al., 2021). Zalles et al. (2021) estimated that 60% of this continent's land surface was impacted by human activities, specially through land use conversion and natural land cover modifications from 1985 to 2018 (e.g. expansion of soybean at the expense of natural habitats including native grasslands and primary forests). In addition, climate projections indicated an expected change in the distribution, frequency and intensity of rainfall with increasing periods of drought and extreme precipitation in this part of the world. As an example, rainfall in southern Chile and southwestern Argentina was shown to have been decreasing since 1960 while at the same time it has been increasing in northwestern Peru and Ecuador (Barros et al., 2014). The occurrence of extreme rainfall events in catchments impacted by land use and cover changes and the intensification and expansion of agricultural practices was shown to accelerate soil erosion and induced deleterious consequences downstream including muddy floods (Evrard et al., 2007; Morera et al., 2017), or an increased transfer of particle-bound contaminants and the siltation of water bodies (Foucher et al., 2021b). The South-American continent is highly dependent on water resources stored in dams for irrigation (with agriculture as the main user), hydroelectric power production (60% of electricity demand supplied by hydroelectric power generation according to the International Energy Agency) and the animal and human food supply (Paredes-Beltran et al., 2021). The siltation of these reservoirs with sediment that may be contaminated with pesticides or other pollutants may impair the quality and quantity of the water resources available, which may lead to multiple deleterious economic, environmental and health consequences (de Campos et al., 2020).

Peru is among the countries that are the most strongly impacted in South America by extreme rainfall events and widespread land cover changes (e.g. deforestation of both humid and dry forests, expansion of agriculture). The climate of the North Peru is highly controlled and influenced by the El Niño-Southern Oscillation (ENSO) involving changes in the temperature of seawater in the central and eastern tropical parts of the Pacific Ocean following a cycle lasting for 3 to 7 years. This oscillation directly affects rainfall distribution in Peru as in other regions of the world. The negative and positive ENSO events are generally defined based on the Southern Oscillation Index (SOI). Negative SOI values indicate the occurrence of strong El Niño events (warm events) with abundant rainfall, whereas positive SOI values refer to La Niña events (cold events). During the recent history (post-1950), several Extreme El Niño Events (EENE: e.g. 1982-1983, 1997-1998) and Coastal El Niño Events (CENE: 2016-2017) were observed with deleterious environmental consequences in Peru (e.g. floods, landslides) and human losses. The EENE recorded in 1997-1998 has induced, for example, more than US$100 million of damage (CTAR, 1998). To adapt to these extreme climatic conditions and alternating dry and wet periods on the Peruvian coast (arid region), farmers used water from reservoirs for irrigation to develop agriculture at the expense of natural vegetation (e.g. dry forest) or implemented large-scale management measures to expand agriculture along the riverine system. This management phase

https://doi.org/10.5194/egusphere-2022-1233
Preprint. Discussion started: 9 December 2022

generated extensive soil disturbance, which may exacerbate the transport of sediment to lower river sections during El Niño events (ENE) (Marin, 2020).

Using data available from a network of river gauging stations, Morera et al. (2017) investigated the impact of EN and EENE on sediment transport along the western Peruvian Andes. They described with a high temporal resolution sediment dynamics during short time periods. Nevertheless, these time series are generally discontinuous (e.g. destruction of the gauging station during extreme events) and sediment properties were rarely characterized.

To overcome these limitations, sediment accumulated in dam reservoirs may provide a powerful alternative for continuously reconstructing sediment properties and dynamics in this region. Although limnogeological studies were widely used for paleoclimatic and paleoenvironmental reconstructions in the Northern Hemisphere (e.g. Alps, Great Lakes of USA), much less studies based on the analysis of lacustrine archives were conducted in the Southern-Hemisphere in general, and in Peru particular (Foucher et al., 2021a). This lack of studies can likely be explained by the low number of freshwater bodies in this region, especially on the western edge of the Andes. Most of the existing limnological studies focusing on EN events were consequently focused on marine sediment cores (Hendy et al., 2015). The relative lack of studies can also be explained by the complexity to date these recent sediment archives (>1950) using radionuclides in this this low-latitude area with limited thermonuclear bomb fallout (Chaboche et al., 2021).

Accordingly, the current research investigated, as a representative study case, the sediment accumulated in the Poechos reservoir (Northern Peru) for retrospectively reconstructing the impact of the ENSO and agriculture expansion along the riverine system of the dry tropical forest biome on sediment dynamics and sources (1978-2019). To this end, a sediment core was dated and characterized by multiple physical and chemical analyses for (1) estimating the evolution of sedimentation rates and (2) identifying the changes in sediment sources associated with the ENE and the agricultural expansion in zones located upstream of the reservoir. The main goal of this study is to improve our understanding of the sedimentary cascade in a region of the world where the sustainability of soil and water resources is of major concern. The identification of sediment sources and their relationship with sediment dynamics can help improving upstream watershed management to limit the adverse effects of accelerated soil erosion on the reservoir siltation.

2 Site and Materials & methods

2.1 Study site

The Catamayo-Chira catchment (15,940 km²) is located in the Northern part of Peru at the boundary with Ecuador (46 and 54% of the catchment surface area are located in Peru and Ecuador, respectively), (Fig. 1). This catchment is characterised by a contrasted relief with a lowland area in the western part and the foothills of the Andean mountains in the eastern part (the west-east gradient ranges from 81 m a.s.l at the catchment outlet to 3958 m a.s.l in the eastern part of the basin). Geology of the catchment is mainly dominated by the occurrence of intrusive rocks from Neocene and Palaeocene (volcanic, granitoid formations) in the Andes (e.g. *Formacion Volcanico Porculla, Volcanico Llama*) and by Upper Cretaceous sedimentary and

https://doi.org/10.5194/egusphere-2022-1233
Preprint. Discussion started: 9 December 2022

Volcanic formations in the lowland area. Two mains ecoregions are found in this basin: The Tumbes-Piura dry forests in the lowland section (dessert area) and the eastern cordillera forest in the upper Andean part. The dominant land cover of the catchment corresponds to agricultural land with 35.2% (4775 km^2) of the catchment area (Fig. 1), it is distributed across the entire catchment, although with a greater presence in the middle and upper parts, where rainfall is more frequent, contrarily to the situation in the lower part, where agriculture is restricted to areas with access to water from rivers or the Poechos reservoir. Numerous different crops are cultivated in the catchment (e.g. rice, cotton, corn, beans, cassava, sweet potatoes, potatoes, coffee, cocoa) (Otivo, 2010). Forty percent of the Economically Active Population of the catchment is linked to agriculture and to extractive activities in the forests (ANA, 2015). The dry forest covers 30.5% (4142 km^2) of the catchment and is mainly found in the lower part of the catchment. This type of land cover is particularly adapted to the regime and amount of rainfall found in this area, and the dry forest is being mainly degraded by the use of wood for firewood, illegal logging and change of land use associated with agriculture expansion (Otivo M. et al., 2014). According to MINAM (2016), on the coast, agriculture with technified irrigation has been reclaiming land from the dry carob forests, and every day a greater number of wooded areas are used for livestock and beekeeping. The herbaceous and/or shrubby vegetation covers 22.4% of the catchment (30322 km^2), mostly in the middle and upper parts of the catchment, in areas where crop establishment is difficult. The forest covers 6.6% of the surface (896 km^2), including natural and non-natural plantations.

This catchment drains into the strategic Poechos reservoir (occupying a surface area of 115 km² during the humid period). This water body located at the catchment outlet was built in 1976 to provide water for local agriculture (approximately 35,000 ha are irrigated), electric power production and to prevent flood risk. This reservoir is supplied by the Chira river (approximately 750 km of river network across the catchment). This reservoir suffers from a continuous reduction of its capacity due to the excessive supply of sediment from the sources located in the vicinity and upstream of the reservoir. The greatest accumulation has occurred during EENE years 1983, 1998 and CENE 2017 when sediment production and transport were found to be greater than during years of average rainfall. A bathymetric study showed that the storage loss in the active volume of the reservoir between 1976 and 1998 was 37.9%, and between 1976 and 2017 the storage loss reached 58.4% (Marin, 2020).

2.2 Materials & methods

2.2.1 Sampling

A 4.5m long sediment core (-80.462745; -4.570902; IGSN number: IEFOU0009) was collected in October 2019 in the upper part of the Poechos reservoir using a COBRA TT vibracorer equipped with 90 mm PVC liners available at the Geophysical Institute of Peru (Fig. 1). This sedimentary sequence was sectioned into six sections for transportation with a length ranging between 51 and 61 cm.

The potential sources of sediment (n=17) were sampled in 2019 for tracing the origin of sediment accumulated in the reservoir. Two main sources were targeted, i.e. the Andean area and the dry forest lowland area, located in the upper and lower parts of

https://doi.org/10.5194/egusphere-2022-1233
Preprint. Discussion started: 9 December 2022

the catchment, respectively (Fig. 1). Source sampling was performed using a metallic trowel and consisted in collecting the uppermost layer of the soil (≈ upper two centimeters).

2.2.2 Laboratory analyses

Sediment core sections were analyzed with an Avaatech X-Ray Fluorescence core scanner (XRF) available at the Laboratoire des Sciences du Climat et de l'Environnement (Gif-sur-Yvette, France) to obtain high resolution (0.5 cm) and semi-quantitative (cps) values of chemical elements along the core. These data were used for characterizing potential changes in sediment sources throughout time associated with land cover and climate changes across the basin. Titanium (Ti), potassium (K), strontium (Sr), rubidium (Rb) and the titanium/calcium ratio (Ca/Ti) were used for identifying potential changes in detritical material contributions along the sequence (Croudace and Rothwell, 2015).

Particle size analysis was performed using a Malvern Mastersizer 3000 allowing to measure the grain size distribution between 10 nm and 3.5 mm. Particle size was measured on the coarser layers identified along the core (n=19) and on randomly selected samples along the sequence (n=10). Grain size parameters such as d10, d50, d90 and raw data were extracted for characterizing these properties.

Non-calibrated sediment density was recorded every 0.6 mm along the sediment sequence using Computer Tomography scanner (CT-Scan) images obtained using the equipment (GE Discovery CT750 HD) available at the DOSEO platform (Université Paris-Saclay, CEA, List). Image reconstruction and relative density values (CT-number) were extracted from the scanner images using the free software ImageJ (Schneider et al., 2012) following the procedure described in Foucher et al. (2020).

Energy dispersive X-ray fluorescence (ED-XRF) measurements (Epsilon 3, Malvern Panalytical) were conducted on selected samples along the sediment cores to obtain concentrations in major elements and calibrate the relative concentrations obtained with the semi-continuous XRF analyses. ED-XRF measurements were conducted on 0.5g of crushed sediment. Calibration was performed using the free software package XELERATE (http://www.ascar.nl/). In addition to the analyses performed on the sediment core, ED-XRF measurements were also conducted on the 17 source samples.

The R package FingerPro was used for estimating the sediment contributions supplied by the potential sources (dry forest vs Andean area) in the sediment accumulated in the reservoir based on the ED-XRF and calibrated XRF records from the sediment sequence. This model un-mixed the sediment sources after a three-step statistical tracer selection procedure described in Lizaga et al. (2020).

2.2.3 Sediment core dating

Core chronology was established by fitting the E (Eastern Pacific) index (E index positive and negative values correspond to warm and cold events, respectively) defined by Takahashi et al. (2011) from monthly Sea Surface Temperature (SST) anomalies for describing the extreme warm events along the north Peruvian coast (this index is available at: http://190.187.237.251/datos/ecindex_ersstv5.txt) with the CT-number extracted from the computer tomography scanner

https://doi.org/10.5194/egusphere-2022-1233
Preprint. Discussion started: 9 December 2022

imageries. Correlation between these temporal series was performed using the updated version of the free software Analyseries (Paillard et al., 1996), Qanalyseries (Kotov and Paelike, 2018).

Age-depth model validation was performed by comparing the sedimentation rate (SR expressed in cm.yr^{-1}) reconstructed by Qanalyseries with the annual volume of sediment accumulated in the reservoir as estimated by annual bathymetric surveys (Marin, 2020). In addition, gamma spectrometry measurements were obtained using HPGe detectors (Canberra/Ortec) available at the Laboratoire des Sciences du Climat et de l'Environnement. Short-lived radionuclides (caesium-137 (^{137}Cs) and excess of lead-210 ($^{210}Pb_{ex}$)) were measured in 12 samples of dry sediment (≈10g) collected along the sedimentary sequence (approximatively every 40 cm).

3 Results

3.1 Core chronology

Correlation between E index and relative density extracted from the sediment core (r^2 of 0.45) was used to provide the chronology of the 19CO3 core. The age-model covered the period ranging between 1978 and 2019, with the lower layer corresponding approximately to the impoundment of the reservoir and the upper layer corresponding to the year of the core sampling, (Fig. 2). No $^{210}Pb_{xs}$ decrease was observed along this sediment core. Values of Lead-210 were ranging between 10 to 6 Bq kg^{-1}, respectively from the top to the bottom of the sequences without any significant decreasing relationship with depth. The artificial ^{137}Cs radionuclide was not detected at all along this sediment core. Consequently, both radionuclides could not be used for the age-model validation.

The highest SR of the 19CO3 core were observed between 1982-1983, 1997-1998, 2008-2009 and 2016-2017 with average SR values of 10, 50, 23 and 31 cm yr^{-1} respectively (Fig. 2). These periods correspond to the historical EENE, ENE and CENE that have led to a significant reduction of the reservoir capacity with the input of large amounts of sediment, respectively 83 million m^3 for the EENE 1982-1983, 75 million m^3 for the EENE 1997-1998, 50 million m^3 for the ENE 2008-2009 and 37 million m^3 for the CENE 2016-2017 (Fig. 2). The identification of these historical EENE, CENE and ENE in the sediment core was used to validate the core chronology. In addition to the increases in SR associated with these events, a general shift in SR was observed in this sequence. An average SR of 5.7 cm yr^{-1} (SD 2.5 cm yr^{-1}) was observed for the 1978-1996 period, whereas a higher mean SR of 13.7 cm yr^{-1} (SD 9 cm yr^{-1}) was found between 1997 and 2019, corresponding to a 140% increase after 1997.

3.2 Lithology

The 19CO3 core was composed of a succession of coarser layers (d50 ranging between 24 and 287 µm) and of finer sediment layers (d50 ≈ 10 µm) in the upper part of the sequence (respectively between 1996 and 2019). In the lower part corresponding to material deposited between 1978 and 1996, fine and homogenous sediment was found (d50 ≈ 9 µm). A total of 19 coarser layers were visually observed in this sequence (Fig. 3 & 4). The main coarser layers were observed in 1997, 2008, 2011 and

https://doi.org/10.5194/egusphere-2022-1233
Preprint. Discussion started: 9 December 2022

2016 with a corresponding thickness of 7.5, 12, 7.5 and 25.5 cm. No such layer was observed before 1996. Thickness, grain size properties and age of these layers are detailed in Table 1.

Changes in geochemical contents such as those shown by Ca/Ti and Sr values highlighted the occurrence of a significant positive trend (Mann Kendall test, *p*-value <0.05) during the 1978-2019 period whereas Ti and K showed a negative trend (*p*-value <0.05). No statistical trend was observed for Rb (*p*-value of 0.3). The highest Ca/Ti and Sr values were recorded between 2007 and 2012 as well as during the 2015-2017 period. Positive fluctuations in Ca/Ti and Sr contents were mainly observed during the positive E index periods whereas the Ti behaviour showed the opposite trend with a decrease in Ti values during the positive E index periods (Fig. 3). The main changes in Ti contents were observed during the 1982-1984, 1991-1992, 1996-1998 and 2016-2017 periods corresponding to EENE, ENE and CENE as well between 2007 and 2012 without any association with EENE or ENE. Finally, the K and Rb contents showed very similar fluctuations (r^2 of 0.73 between both elements) (Fig. 4).

3.3 Sediment sources

Two tracing properties (K and Rb) were selected by the FingerPro statistical procedure for un-mixing the sediment source contributions along the 19C03 sequence (Fig. 5). K content ranged between 0.6 and 2.25% in the soil samples. The highest K contents were measured in the Andean potential sediment sources with an average value of 1.5% (SD 0.4%, ranging between 0.9 and 2.2%) whereas a lower average value of 0.9% (SD 0.2%, ranging between 0.6 and 1.2%) was recorded in the lowland dry forest source. A similar trend was observed for the Rb content with the highest values measured in the upstream sources (0.07%, SD 0.01%, ranging between 0.06 and 0.1%) and the lowest values in the downstream source (0.05%, SD 0.01%, ranging between 0.03 and 0.06%).

Calibrated K values from the sediment core (r^2 of 0.92 between XRF and ED-XRF calibration) varied between 0.7 and 1.8% with an average value of 1.1% (SD 0.15%). The average calibrated Rb value (r^2 of 0.8 between XRF and ED-XRF calibration) reached 0.05% (SD 0.01%) with values ranging between 0.03 and 0.12% (Fig. 5).

FingerPro results showed that 31% (SD 22%) of the sediment accumulated in the core was originating from the Andean source, while 69% (SD 22%) of the material was supplied by the lowland dry forest source (Fig. 6). According to the Mann-Kendall test, the sediment contribution of the dry forest followed a positive trend between 1978 and 2019 (*p*-value <0.05). On average, the dry forest source contributed 76% (SD 20%) of the sediment accumulated in the reservoir during the positive E index phases. During the negative E index periods, Andean source contribution increased and supplied 40% (SD 22%) of the material accumulated in the reservoir.

The contribution of the dry forest sources during the EENE1982-1983, 1997-1998 and CENE2016-2017 reached 94% (SD 4%), 65% (SD 25%) and 90% (SD 9%), respectively.

https://doi.org/10.5194/egusphere-2022-1233
Preprint. Discussion started: 9 December 2022

4 Discussion

Fallout radionuclide measurements could not be used for the establishment of the core chronology due to the low activities of $^{210}Pb_{ex}$ and the absence of ^{137}Cs in the core sediment. Past studies had demonstrated the low ^{137}Cs activities found in soils and sediment in this low-latitude region of South-America (Chaboche et al., 2021) whereas the $^{210}Pb_{ex}$ was supposed to be present in the upper part of the soil (≈5cm) before decreasing with depth. The very low lead-210 activities detected in the sediment core can provide information on the intensity of erosion processes in this region by mobilizing subsoil sources (channel bank, gullies) depleted in $^{210}Pb_{ex}$, and consequently highly impacted by erosion processes (Evrard et al., 2020).

The sedimentary sequence of the Poechos reservoir recorded two contrasted phases of sediment transfers associated with changes in climate and human activities. Before 1997, the sedimentation rate recorded in the reservoir remained mainly constant (5.7 cm yr^{-1}, SD 2.5 cm yr^{-1}) with the exception of the EENE of 1982-1983 (10 cm yr^{-1}), which was characterized by an acceleration of SR during this humid period (Fig. 2). The absence of coarser material layers during the EENE 1982-1983 and the absence of significant change in detritical proxies (Sr, Ca/Ti) between 1978 and 1996 suggest a period of less intense hydrosedimentary dynamics (Fig. 3) at the coring site. Source apportionment during this first phase underlines a succession of sediment supplies originating from the Andean source during the dry periods and a greater contribution of the lowland dry forest during the humid periods (Fig. 6). This source apportionment is mainly controlled by the rainfall distribution, which is in turn controlled by the prominent topography of the Andean mountains and the interaction between atmospheric moisture flux and orography (Rau et al., 2017). On the dry western flank of Peruvian Andes, mean annual rainfall is estimated to reach 10-15 mm yr^{-1} below 500 m a.s.l (90 mm yr^{-1} in the Northern Pacific coast, dry forest area) whereas annual rainfall can exceed 1000 mm yr^{-1} around 1000 and 3000 m a.s.l on the western side of the Peruvians Andes (Arias et al., 2021). ENE, EENE and CENE associated with warm temperatures along the Peruvian coast (positive E index) disrupt this rainfall pattern with heavy precipitation occurring on the western dry flank of Peruvian Andes along the lowland areas occupied by the dry forest characterized by a low vegetation cover prone to erosion. Rainfall in Piura City, located to the south of the Poechos reservoir amounts to 60 mm yr^{-1} during a normal year whereas during the EENE of 1982-1983 and 1997-1998, annual rainfall of 2150 and 1800 mm yr^{-1} was recorded (Takahashi, 2004). This climatic specificity influenced by ENSO therefore explains the contrasted source contributions observed in the Poechos reservoir during the warm and cold phases.

A significant acceleration of sediment delivery was observed during the 1990s with the occurrence of a tipping point just before the EENE 1997-1998. From this period onwards, sedimentation rate increased by 140% (Fig. 2 & 6). The Poechos reservoir is surrounded by rivers mainly located in Peru (dry forest biome), with low baseflow of +-10 L/s during the dry season. The occurrence of a low but permanent flow in an arid region makes agricultural practices possible. For this reason, the inhabitants, mostly farmers, took possession of the floodplain for agriculture development during the last several decades. Each section and stretch of the river was assigned an owner, taking charge of delineating his property every year when the level of the river allows it. Depending on rainfall and hydrological characteristics (El Niño or La Niña events and their respective intensity) and associated sediment transport, sediment quantity available in the floodplain may be insufficient to

https://doi.org/10.5194/egusphere-2022-1233
Preprint. Discussion started: 9 December 2022

conduct farming. In this situation, farmers used heavy machinery to transport soil and sediment material from nearby rivers or hillsides in order to provide sufficient substrate for planting crops requiring a short vegetative period (e.g. vegetables). The construction of the Poechos reservoir generated a wider water channel which was used for agriculture, with crops planted directly on the river bed with some land filling on the slopes to create an optimal area for the farming activity.

In this way, year after year, the population substantially increased the availability of sediments in the main channel of the rivers. In addition, human activity is responsible for making large volumes of sediment available for transport to the Poechos reservoir during the first floods of the wet periods. Due to the stationarity of rainfall, the process is repeated annually, progressively raising the topographic level of the riverbed and generating more sediment transport both by river dredging and soil levelling by farmers. This agricultural practice associated with the occurrence of intense ENE, EENE and CENE after the mid of 1990s may explain the acceleration of sedimentation rates and the greater contribution of the dry forest source to the reservoir siltation. Other processes that took place in the upper basin and associated with tree logging to develop agriculture or to exploit wood (Morocho, 2004) which increased in recent years can also explain a part of these accelerated sediment dynamics.

The greater connectivity and the acceleration of hydrosedimentary dynamics increased the deposition of coarser particles in the reservoir, which is reflected by the change in particle size observed in the investigated core. These coarser layers were associated with the occurrence of major EENE. Before 1997, the EENE and ENE were not specifically associated with the deposition of coarser particles. Of note, the thickness of these layers increased by 220% (moving from a thickness of 7.5 to 24 cm) from the EENE 1997-1998 (first layer observed) to the CENE 2016-2017 (last extreme event layer detected) while the average grain size increased by 190% between both events probably in response to the progressive aggradation of the delta at the coring site.

The Poechos reservoir provides a representative illustration on how water bodies may be impacted by widespread changes in land covers associated with human activities and climate modifications. Marin, (2020) demonstrated than in 41 years (1976-2017), the Poechos dam lost 58.5% of its original storage capacity and that just two major ENSO periods have contributed to 49% of the dam siltation observed between 1976 and 2005 (Tote et al., 2011). This filling rate could further increase in the coming years if the agriculture expansion on the dry forest biome continues to increase and if ENSO events become more frequent and intense under the effect of climate change (Barros et al., 2014). The case of the Poechos catchment is not unique although exemplative of large scale changes in land use (16,000 km²), given the immense volume of sediment transported compared to the size of the reservoir storage capacity ($1000x10^6m^3$). Other examples of severe dam siltation were observed all around the world as in Africa or in India although in general in smaller reservoirs (e.g. storage capacity of $17x10^6m^3$) draining more restricted areas affected by land use changes (136 km²) (e.g. Adongo et al., 2014). This study therefore demonstrates the vulnerability of the Andean region in comparison to other regions of the world to both climate change and the alarming ongoing land use changes. As the world's population is projected to continue to increase in the coming decades, a better management of water and soil resources will be of paramount importance to protect soil and water resources, in terms of both quality and quantity. The identification of sediment sources and their relationship with sediment dynamics can improve

https://doi.org/10.5194/egusphere-2022-1233
Preprint. Discussion started: 9 December 2022

land and river management of upper basin areas to limit the adverse effects of accelerated erosion on reservoir siltation through the design of efficient landscape management strategies.

5 Conclusions

This study highlights the potential of sediment cores for retrospectively reconstructing the interactions between El Niño-Southern Oscillation and the change in agricultural practices on the siltation of reservoirs, with the example of the Poechos Reservoir, Northern Peru (1978-2019). The current study demonstrated the strong relationship between the humid and dry phases of ENSO with the mobilization of different sources of sediment. The occurrence of stationary rainfall during the ENE, EENE and CENE increased the sediment contribution of the dry forest source, a biome characterized by a poor vegetation cover of the soil, which is therefore particularly exposed to erosion. The development of agriculture during the 1990s along the dry forest riverine system amplified sediment transport by dramatically increasing the connectivity between the potential sources of sediment and the reservoir.

As climate changes and agriculture expansion are both expected to continue to increase in the coming decades in South-America generally and in Peru in particular, the lifespan of this reservoir is threatened over the short term as well as the whole of the socio-economic activities which depend on it. It is therefore crucial to improve land management across the basin to contribute to the slowing-down of the sediment cascade dynamics in this fragile environment.

Author contribution

J.M, M.S and J.O have collected the sediment core. A.F has performed the analyses described in this manuscript. A.F, O.E, J.M, M.S and J.O have participed to the results discussion and drafted the main manuscript.

Competing interest

The authors declare that they have no conflict of interest

Acknowledgements

The authors are grateful to the DOSEO platform (Université Paris-Saclay, CEA, List) and especially to Anne-Catherine Simon and Mathieu Agelou for performing the tomography scanner measurements on the core sections. This work was supported by ANR PIA (funding ANR-20-IDEES-0002) and by ProCiencia (https://prociencia.gob.pe) through the project “Implementación del sistema de Monitoreo de los Sedimentos Ante los Riesgos y Desastres”, contract N°011-2018-FONDECYT/BM-Mejoramiento de infraestructura para la investigación, as well as the FONDES project through the “Fortalecimiento de la red de monitoreo de sedimentos y la sedimentación en los embalses de Poechos y Gallito Ciego” and the Technical Cooperation

https://doi.org/10.5194/egusphere-2022-1233
Preprint. Discussion started: 9 December 2022

Project RLA-5076: “Strengthening Surveillance Systems and Monitoring Programmes of Hydraulic Facilities Using Nuclear Techniques to Assess Sedimentation Impacts as Environmental and Social Risks”. It inspired the AVATAR project (ANR-22-CE93-0001) funded by ANR (France) and SNF (Switzerland). In addition, we would like to thank the Proyecto Especial Chira Piura for having provided valuable information for our study.

References

Adongo, T. A., Kugbe, J. X. and Gbedzi, V. D.: International Journal of Science and Technology Siltation of the Reservoir of Vea Irrigation Dam in the Bongo District of the Upper East Region, Ghana, , (12) [online] Available from: http://www.ejournalofsciences.org, 2014.

ANA: Plan de Gestión de los Recursos Hídricos de la Cuenca Chira-Piura, Lima, PE., 2015.

Arias, P. A., Garreaud, R., Poveda, G., Espinoza, J. C., Molina-Carpio, J., Masiokas, M., Viale, M., Scaff, L. and van Oevelen, P. J.: Hydroclimate of the Andes Part II: Hydroclimate Variability and Sub-Continental Patterns, Front. Earth Sci., 8, doi:10.3389/FEART.2020.505467/PDF, 2021.

Barros, V. R., Field, C. B., Dokken, D. J., Mastrandrea, M. D., Mach, K. J., Bilir, T. E., Chatterjee, M., Ebi, K. L., Estrada, Y. O., Genova, R. C., Girma, B., Kissel, E. S., Levy, A. N., MacCracken, S., Mastrandrea, P. R. and White, L. L.: Climate change 2014 impacts, adaptation, and vulnerability Part B: Regional aspects: Working group ii contribution to the fifth assessment report of the intergovernmental panel on climate change, Clim. Chang. 2014 Impacts, Adapt. Vulnerability Part B Reg. Asp. Work. Gr. II Contrib. to Fifth Assess. Rep. Intergov. Panel Clim. Chang., 1–1820, doi:10.1017/CBO9781107415386, 2014.

de Campos Júnior, Araújo, Souto, Campos and Pereira: Contamination and health risks assessment in a dam in the southeast region of Brazil using ecotoxicological methods, J. Toxicol. Environ. Heal. Part A, 83(10), 404–411, doi:10.1080/15287394.2020.1767250, 2020.

Chaboche, P.-A., Saby, N. P. A., Laceby, J. P., Minella, J. P. G., Tiecher, T., Ramon, R., Tassano, M., Cabral, P., Cabrera, M., da Silva, Y. J. A. B., Lefevre, I. and Evrard, O.: Mapping the spatial distribution of global 137Cs fallout in soils of South America as a baseline for Earth Science studies, Earth-Science Rev., 214(August 2020), 103542, doi:10.1016/j.earscirev.2021.103542, 2021.

Croudace, I. W. and Rothwell, R. G.: Micro-XRF Studies of Sediment Cores, edited by I. W. Croudace and R. G. Rothwell, Springer Netherlands, Dordrecht., 2015.

Evrard, O., Bielders, C. L., Vandaele, K. and van Wesemael, B.: Spatial and temporal variation of muddy floods in central Belgium, off-site impacts and potential control measures, CATENA, 70(3), 443–454, doi:10.1016/j.catena.2006.11.011, 2007.

Evrard, O., Chaboche, P.-A., Ramon, R., Foucher, A. and Laceby, J. P.: A global review of sediment source fingerprinting research incorporating fallout radiocesium (137Cs), Geomorphology, 362, 107103, doi:10.1016/j.geomorph.2020.107103, 2020.

https://doi.org/10.5194/egusphere-2022-1233
Preprint. Discussion started: 9 December 2022

Foucher, A., Evrard, O., Cerdan, O., Chabert, C., Lecompte, F., Lefèvre, I., Vandromme, R. and Salvador-Blanes, S.: A quick and low-cost technique to identify layers associated with heavy rainfall in sediment archives during the Anthropocene, Sedimentology, 67(1), 486–501, doi:10.1111/sed.12650, 2020.

Foucher, A., Chaboche, P., Sabatier, P. and Evrard, O.: A worldwide meta-analysis (1977 – 2020) of sediment core dating using fallout radionuclides including 137Cs and 210Pbxs, Earth Syst. Sci. Data, 13, 4951–4966, doi:10.5194/essd-13-4951-2021, 2021a.

Foucher, A., Evrard, O., Cerdan, O., Chabert, C., Lefèvre, I., Vandromme, R. and Salvador-Blanes, S.: Deciphering human and climatic controls on soil erosion in intensively cultivated landscapes after 1950 (Loire Valley, France), Anthropocene, 34, 100287, doi:10.1016/j.ancene.2021.100287, 2021b.

Hendy, I. L., Napier, T. J. and Schimmelmann, A.: From extreme rainfall to drought: 250 years of annually resolved sediment deposition in Santa Barbara Basin, California, Quat. Int., 387, 3–12, doi:10.1016/j.quaint.2015.01.026, 2015.

Kotov, S. and Paelike, H.: QAnalySeries – a cross-platform time series tuning and analysis tool, [online] Available from: https://agu.confex.com/agu/fm18/meetingapp.cgi/Paper/349843, 2018.

Lizaga, I., Latorre, B., Gaspar, L. and Navas, A.: FingerPro: an R Package for Tracking the Provenance of Sediment, Water Resour. Manag., 34(12), 3879–3894, doi:10.1007/s11269-020-02650-0, 2020.

Marin Alvarez Yasmin, E.: CUANTIFICACIÓN Y CLASIFICACIÓN DE LAS TASAS DE SEDIMENTACIÓN EN EL RESERVORIO POECHOS, Piura., 2020.

MINAM: Identificación de condiciones de riesgos de desastres y vulnerabilidad al cambio climático en la Región de Piura., 2016.

Morera, S. B., Condom, T., Crave, A., Steer, P. and Guyot, J. L.: The impact of extreme El Niño events on modern sediment transport along the western Peruvian Andes (1968-2012), Sci. Rep., 7(1), 1–14, doi:10.1038/s41598-017-12220-x, 2017.

Morocho Calle, F.: Estudio “Sedimentación del reservorio de Poechos y recuperación de volumen de agua de regulación para sistema Chira-Piura.”, 2004.

Otivo, J. .: Memoria descriptiva: Mapa de ocupación del terriotrio y uso actual del suelo., 2010.

Otivo M., J., Otivo B., J. and Llanos A., M.: Análisis de la cobertura vegetal y la degradación del bosque tropical estacionalmente seco en el Distrito de Lancones, Sullana, Piura. [online] Available from: https://repositoriodigital.minam.gob.pe/handle/123456789/503, 2014.

Paillard, D., Labeyrie, L., Yiou, P., Paillard, D., Labeyrie, L., Yiou, P. and Program, M.: Macintosh Program performs time-series analysis, vol. 77, edited by A. G. U. (AGU) Eos, Transactions American Geophysical Union, pp. 379–379., 1996.

Paredes-Beltran, B., Sordo-Ward, A. and Garrote, L.: Dataset of Georeferenced Dams in South America (DDSA), Earth Syst. Sci. Data, 13(2), 213–229, doi:10.5194/essd-13-213-2021, 2021.

Rau, P., Bourrel, L., Labat, D., Melo, P., Dewitte, B., Frappart, F., Lavado, W. and Felipe, O.: Regionalization of rainfall over the Peruvian Pacific slope and coast, Int. J. Climatol., 37(1), 143–158, doi:10.1002/joc.4693, 2017.

Schneider, C. A., Rasband, W. S. and Eliceiri, K. W.: NIH Image to ImageJ: 25 years of image analysis, Nat. Methods, 9(7),

https://doi.org/10.5194/egusphere-2022-1233
Preprint. Discussion started: 9 December 2022

671–675, doi:10.1038/nmeth.2089, 2012.

Song, X.-P., Hansen, M. C., Potapov, P., Adusei, B., Pickering, J., Adami, M., Lima, A., Zalles, V., Stehman, S. V., Di Bella, C. M., Conde, M. C., Copati, E. J., Fernandes, L. B., Hernandez-Serna, A., Jantz, S. M., Pickens, A. H., Turubanova, S. and Tyukavina, A.: Massive soybean expansion in South America since 2000 and implications for conservation, Nat. Sustain., 4(9), 784–792, doi:10.1038/s41893-021-00729-z, 2021.

Takahashi, K.: The atmospheric circulation associated with extreme rainfall events in Piura, Peru, during the 1997--1998 and 2002 El Niño events, Ann. Geophys., 22(11), 3917–3926, doi:10.5194/angeo-22-3917-2004, 2004.

Takahashi, K., Montecinos, A., Goubanova, K. and Dewitte, B.: ENSO regimes: Reinterpreting the canonical and Modoki El Nio, Geophys. Res. Lett., 38(10), doi:10.1029/2011GL047364, 2011.

Tote, C., Govers, G., Van Kerckhoven, S., Filiberto, I., Verstraeten, G. and Eerens, H.: Effect of ENSO events on sediment production in a large coastal basin in northern Peru, Earth Surf. Process. Landforms, 36(13), 1776–1788, doi:10.1002/esp.2200, 2011.

Winkler, K., Fuchs, R., Rounsevell, M. and Herold, M.: Global land use changes are four times greater than previously estimated, Nat. Commun. 2021 121, 12(1), 1–10, doi:10.1038/s41467-021-22702-2, 2021.

Zalles, V., Hansen, M. C., Potapov, P. V., Parker, D., Stehman, S. V., Pickens, A. H., Parente, L. L., Ferreira, L. G., Song, X. P., Hernandez-Serna, A. and Kommareddy, I.: Rapid expansion of human impact on natural land in South America since 1985, Sci. Adv., 7(14), doi:10.1126/SCIADV.ABG1620/SUPPL_FILE/ABG1620_SM.PDF, 2021.

https://doi.org/10.5194/egusphere-2022-1233
Preprint. Discussion started: 9 December 2022

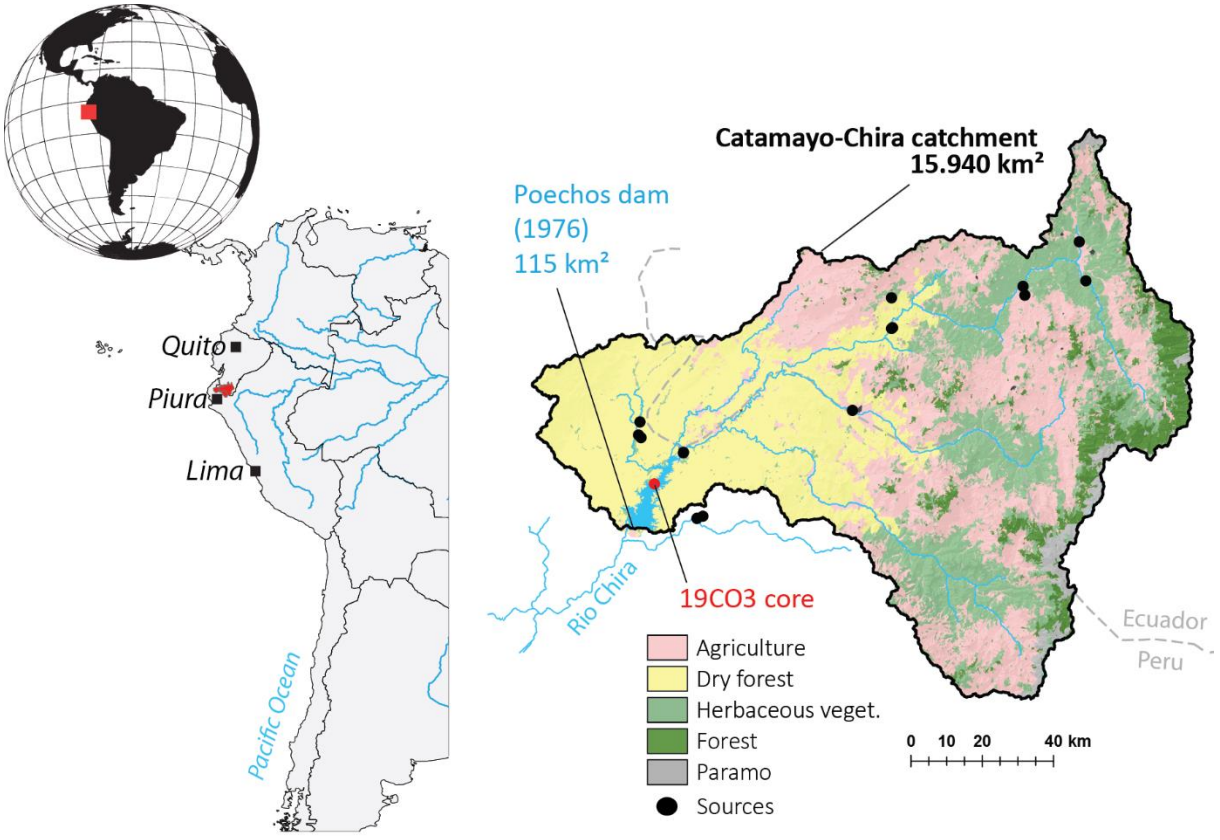

405 **Fig. 1 Left- Regional location of the Catamayo-Chira Basin along the western Andes at the boundary between Ecuador and Peru (SRTM digital elevation (USGS, 2018)). Right – general setting of the Catamayo-Chira Basin with the simplified land cover 2016 base**

410

https://doi.org/10.5194/egusphere-2022-1233
Preprint. Discussion started: 9 December 2022

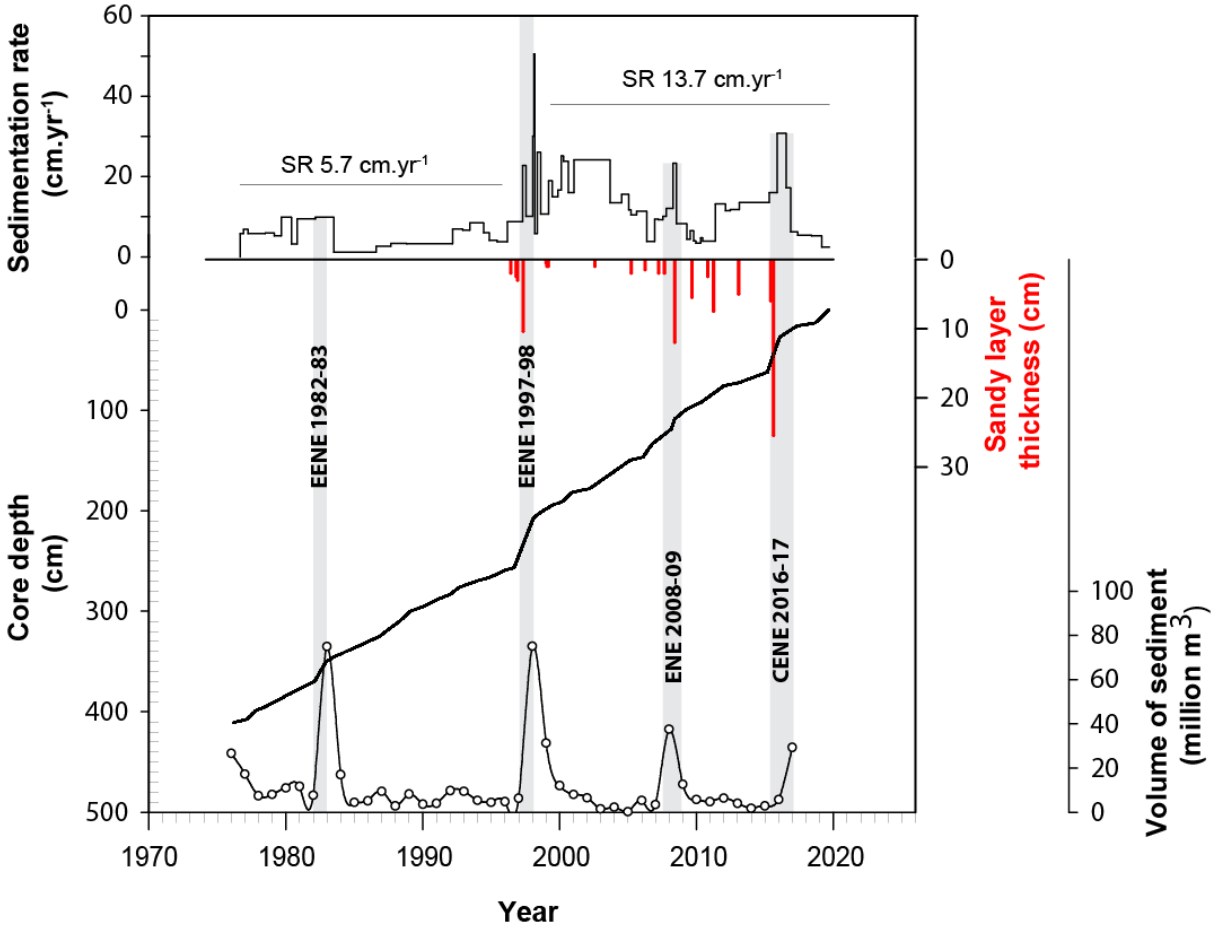

Fig. 2 Core chronology of the 19C03 core established after correlation between the CT-number and the Eastern Pacific Index (SR=sedimentation rate)

https://doi.org/10.5194/egusphere-2022-1233
Preprint. Discussion started: 9 December 2022

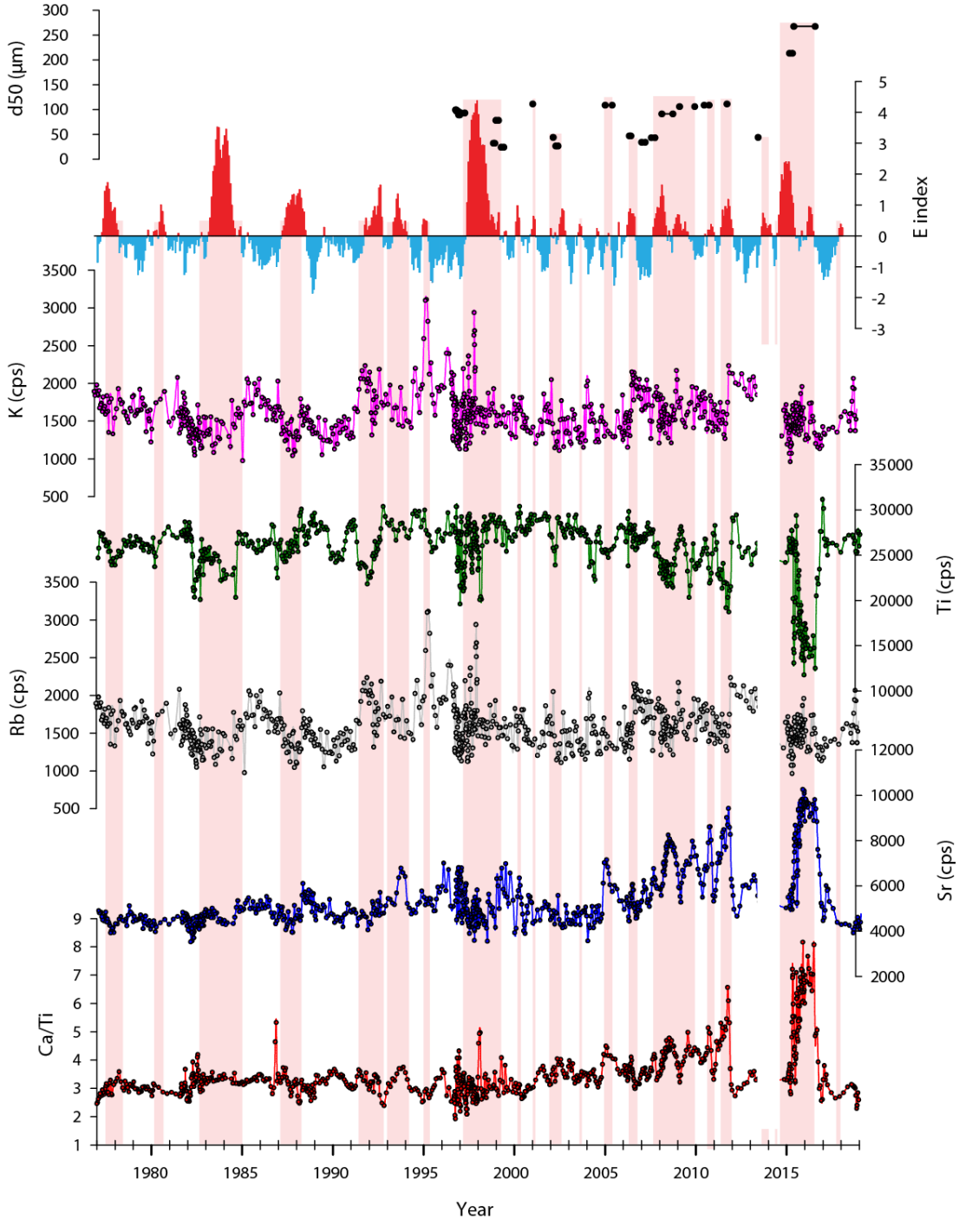

Fig. 3 Evolution of sediment properties (chemical elements analysed with an XRF core scanner) along the 19C03 core

https://doi.org/10.5194/egusphere-2022-1233
Preprint. Discussion started: 9 December 2022

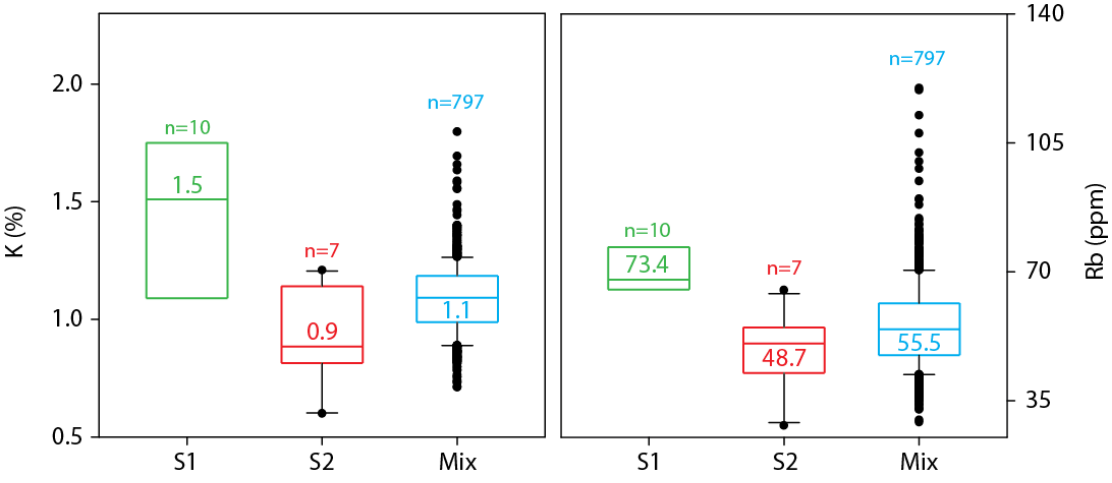

420 **Fig 4 Boxplot of the selected tracer properties (K and Rb) in both the sediment target samples and the potential sources (S1 and S2 correspond respectively to the Andean mountains and the Lowland dry forest sources)**

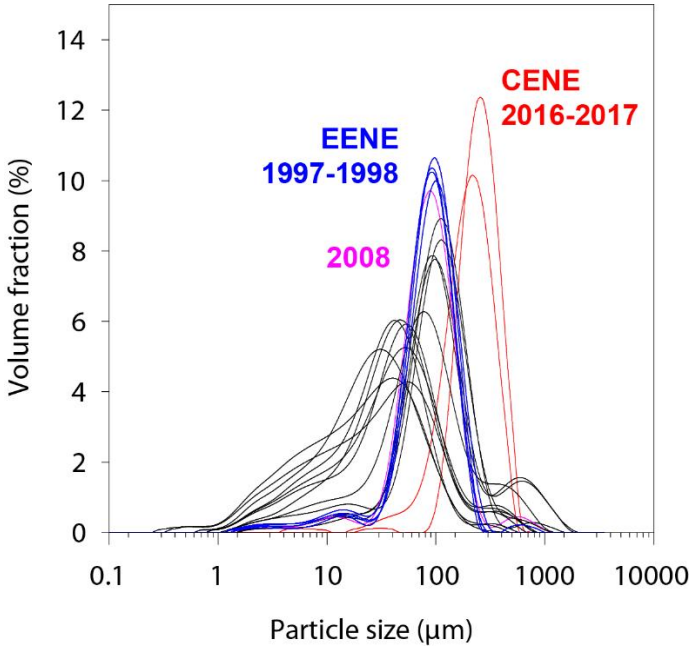

425 **Fig. 5 Particle size distributions of the 19 coarser layers detected in the 19CO3 core (EENE: Extreme El Niño Event, CENE: Coastal El Niño Event)**

https://doi.org/10.5194/egusphere-2022-1233
Preprint. Discussion started: 9 December 2022

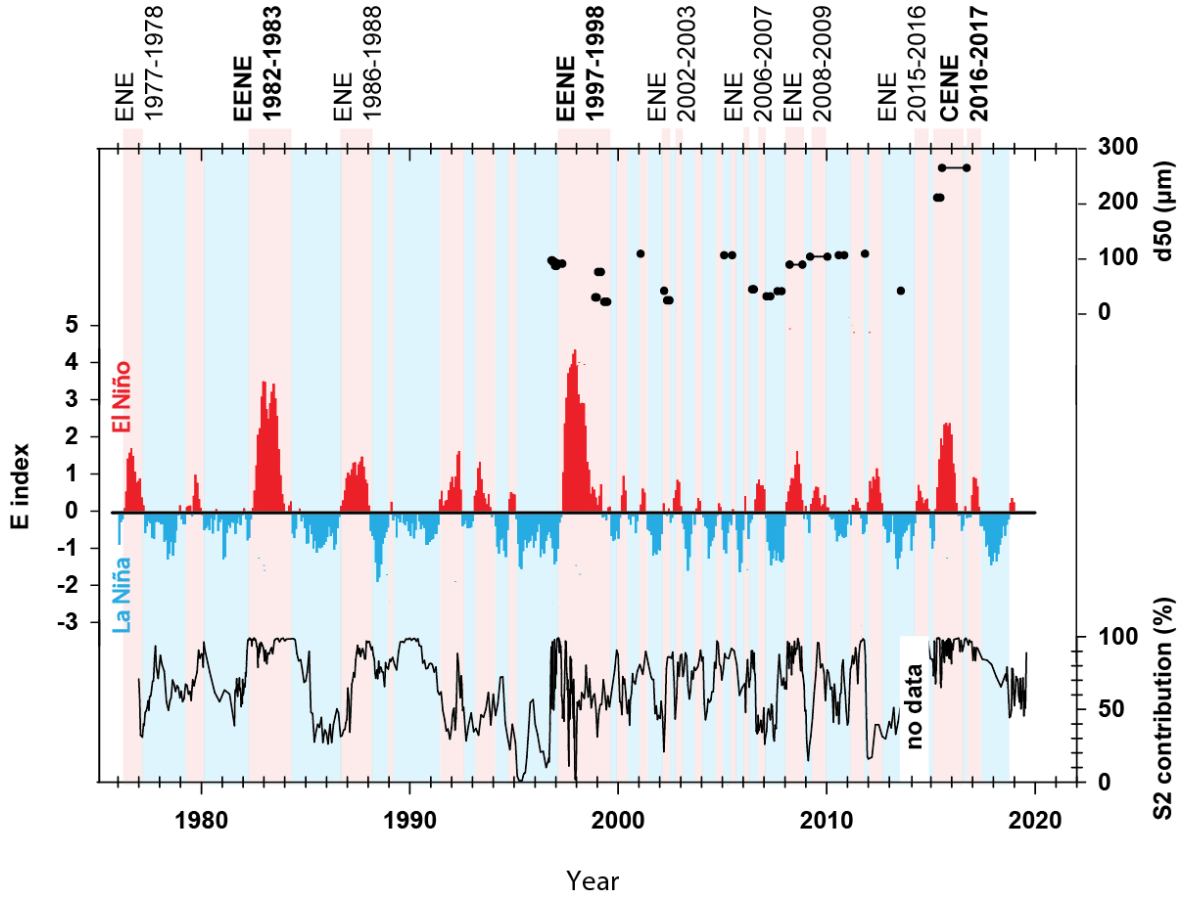

Fig 6. Comparison between sediment sources (S2 contribution = lowland dry forest source), E index (East Pacific Index) and the 19 coarser sediment layers identified along the 19CO3 core.

https://doi.org/10.5194/egusphere-2022-1233
Preprint. Discussion started: 9 December 2022

Table 1 Properties of the 19 coarser layers identified in the 19CO3 sediment core

layer ID	min Depth (cm)	max Depth (cm)	Thickness (cm)	Min Age	Max Age	d10	SD	d50	SD	d90	SD
1	21	46.5	25,5	2016,7	2015,5	158	0.2	267	0.5	439	1.8
2	49.5	55.5	6	2015.4	2015.3	99	0.3	213	0.5	381	1.1
3	70	75	5	2013.5	2002.2	10	0.2	44	0.6	131	5.4
4	77.5	85	7.5	2011.8	2001.0	46	0.5	111	0.4	225	1.8
5	87.5	90	2.5	2010.8	2010.5	41	1.2	109	2.1	490	84.0
6	94	99.5	5.5	2010.0	2009.2	43	1.0	106	2.0	521	77.3
7	103.5	11.,5	12	2008.8	2008.2	43	0.1	91	0.2	178	1.6
8	122	124	2	2007.8	2007.6	6	0.1	43	0.3	144	3.1
9	128	130	2	2007.3	2007.1	6	0	34	0.1	91	0.4
10	139	140,5	1.5	2006.5	2006.4	7	0.1	47	0.5	144	4.8
11	149	151	2	2005.4	2005.1	19	0.6	109	0.4	234	2.4
12	172.5	173.5	1	2002.4	2002.3	5	0	27	0.2	83	0.9
13	195	196	1	1999.4	1999.3	3	0	24	0.1	87	0.6
14	197	198	1	1999.1	1999.0	14	0.5	78	1.2	300	29.8
15	198.5	199	0.5	1998.9	1998.9	4	0.1	32	1.0	126	3.2
16	234.5	242	7.5	1997.3	1997.1	44	0.3	93	0.1	169	0.6
17	244	247	3	1997.0	1996.9	36	0.6	89	0.4	159	1.1
18	248	250.5	2.5	1996.9	1996.8	47	0.2	97	0.2	169	0.9
19	251	253	2	1996.8	1996.8	42	0.2	99	0.1	181	0.3